Supplemental Materials for "Electron-Correlation-Induced Charge Density Wave in FeGe"

Lin Wu,* Yating Hu,* Dongze Fan, Di Wang,† and Xiangang Wan‡
National Laboratory of Solid State Microstructures and School of Physics, Nanjing University, Nanjing 210093, China and Collaborative Innovation Center of Advanced Microstructures, Nanjing University, Nanjing 210093, China

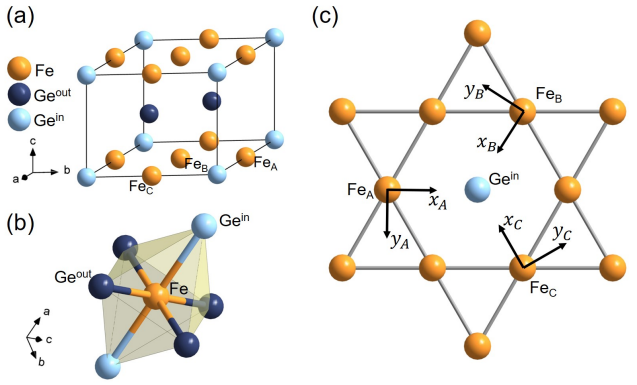

FIG. S1. (a)The crystal structure of FeGe. The light blue, dark blue, and orange spheres represent Ge^{in}, Ge^{out}, and Fe atoms, respectively. The Fe atoms located at three different sites are labeled as Fe_A, Fe_B, and Fe_C. (b) The local structure of the $FeGe_6$ octahedron. The octahedron includes two Ge^{in} atoms and four Ge^{out} atoms. (c) Our local coordinate for each Fe atom. The local x-axis always points to the nearest-neighbor Ge^{in} atom, and the z-axis of each local coordinate is perpendicular to the paper surface.

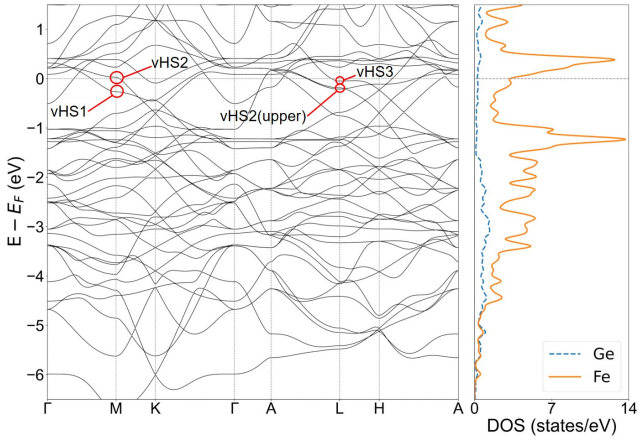

FIG. S2. Band structure (left panel) and DOS (right panel) of A-type AFM FeGe. The Fermi level is aligned to 0eV. The DOS of Fe-3d orbitals and Ge-4p orbitals are indicated by the solid orange and dashed blue lines, respectively.

A. Crystal Structure

Hexagonal FeGe is an intermetallic compound of the CoSn structure and crystallize into the $P6/mmm$ (No. 191) space group[1]. As shown in Fig. S1(a), there are two distinct types of Ge atoms in a unit cell, labeled Ge^{in} (site 1a) and Ge^{out} (site 2d) respectively, depending on whether they are on the same layer as Fe atoms. In the Fe-Ge^{in} plane, three Fe atoms at different sites (noted as Fe_A, Fe_B, and Fe_C in Fig. S1(a)) form Kagome lattices, and Ge^{in} atoms are located in the center of the hexagons. Ge^{out} atoms compose honeycomb structures above and below the Fe-Ge^{in} plane.

The local structure of the $FeGe_6$ octahedron is shown in Fig. S1(b). It can be seen that each Fe atom is surrounded by six Ge atomic octahedrons, including two Ge^{in} atoms and four Ge^{out} atoms. In the O_h crystal field, ortho-octahedral structure leads to $t_{2g} - e_g$ energy splitting. Here the octahedron is distorted and induces further splitting of the five Fe-3d orbitals.

B. Band structure and density of states

We perform LSDA calculation for FeGe based on the experimental A-type AFM ground state [2], and show the band structure and the DOS in Fig. S2. As shown in Fig. S2, it is clear that the Fe-3d orbitals dominate the DOS around E_F (-2 to 2 eV relative to E_F), while the Ge-4p orbitals are mainly located between -6.0 and -2.0 eV. In the AFM phase, there is an upshift of the spin minority bands due to the exchange splitting induced by the ordered moment. Two peaks located near 0.4 and -1.3 eV correspond to the flat bands of the spin minority and spin majority states, respectively. The contribution of the Fe-3d and Ge-4p orbitals is relatively close in the range from -6 to -4 eV, suggesting hybridization between the Fe-3d and Ge-4p orbitals.

C. Nesting functions after Fermi surface shift

Compared to the energy band structure obtained from the DFT calculations, the measured dispersion has to be renormalised by multiplication with a factor [3]. In order to consider the effect of the renormalization of the energy band dispersion on the Fermi surface nesting, we give the results of the nesting function $\xi(q_x, q_y, 0)$ in Fig. S3, where the Fermi energy is shifted from E_F-0.1 eV to E_F+0.1 eV. It can be seen that when the Fermi level is shifted, the maximum values of the nesting function are still located at the K point, although the distribution and values of the nesting functions are partially changed. This means that the nesting function calculated from the eigenvalues is robust to the band renormalization.

* These authors contributed equally to this work.
† diwang0214@nju.edu.cn
‡ xgwan@nju.edu.cn

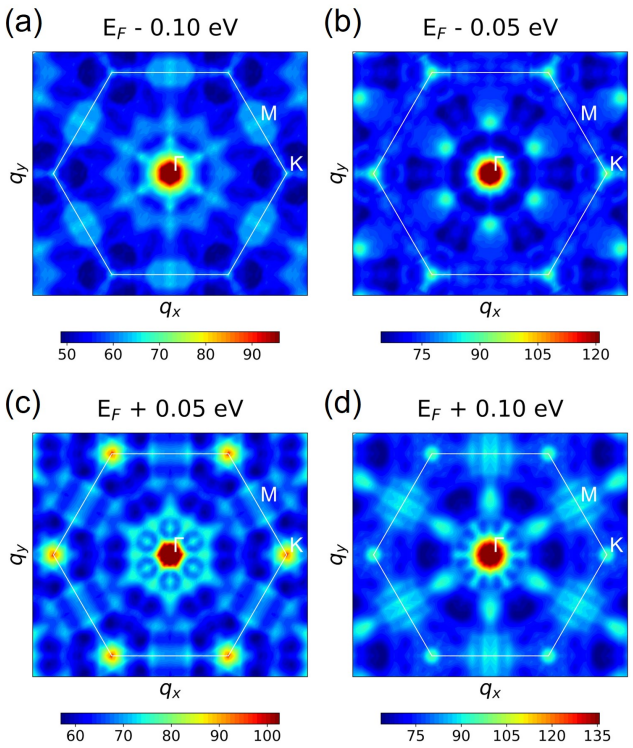

FIG. S3. The nesting function $\xi(q_x, q_y, 0)$ of FeGe, where the Fermi energy is set to (a)E_F-0.1 eV, (b)E_F-0.05 eV, (c)E_F+0.05 eV, and (d)E_F+0.1 eV, respectively. We neglected the peak at q=0 to better present the nesting function.

D. The computational parameters in EPC calculations

The phonon dispersion and electron-phonon coupling (EPC) calculations are performed within density-functional perturbation theory [4] as implemented in the Quantum-ESPRESSO package (QE) [5, 6]. The cutoffs of plane-wave basis set are set to 130 Ry and 520 Ry for the wave functions and the charge density, respectively. The lattice constants are fully relaxed until the force on each atom less than 10^{-5} Ry/$\mathring{A}$, and the convergence criterion for self-consistent calculation is 10^{-9} Ry. The Methfessel-Paxton smearing [7] is set to 0.01 Ry, while the $16 \times 16 \times 8$ k-point mesh is used for EPC calculations.

[1] T. Ohoyama, K. Kanematsu, and K. Yasukōchi, "A New Intermetallic Compound FeGe," J. Phys. Soc. Jpn. **18**, 589–589 (1963).

[2] J. Bernhard, B. Lebech, and O. Beckman, "Magnetic phase diagram of hexagonal FeGe determined by neutron diffraction," J. Phys. F: Metal Phys. **18**, 539 (1988).

[3] X. Teng, J. S. Oh, H. Tan, L. Chen, J. Huang, B. Gao, J.-X. Yin, J.-H. Chu, M. Hashimoto, D. Lu, C. Jozwiak, A. Bostwick, E. Rotenberg, G. E. Granroth, B. Yan, R. J. Birgeneau, P. Dai, and M. Yi, "Magnetism and charge density wave order in kagome fege," Nature Physics , https://doi.org/10.1038/s41567–023–01985–w (2023).

[4] S. Baroni, S. De Gironcoli, A. Dal Corso, and P. Giannozzi, "Phonons and related crystal properties from density-functional perturbation theory," Rev. Mod. Phys. **73**, 515–562 (2001).

[5] P. Giannozzi, S. Baroni, N. Bonini, M. Calandra, R. Car, C. Cavazzoni, D. Ceresoli, G. L. Chiarotti, M. Cococcioni, I. Dabo, A. D. Corso, S. de Gironcoli, S. Fabris, G. Fratesi, R. Gebauer, U. Gerstmann, C. Gougoussis, A. Kokalj, M. Lazzeri, and L. Martin-Samos et al., "Quantum espresso: a modular and open-source software project for quantum simulations of materials," J. Phys.: Condens. Matter. **21**, 395502 (2009).

[6] P. Giannozzi, O. Andreussi, T. Brumme, O. Bunau, M. B. Nardelli, M. Calandra, R. Car, C. Cavazzoni, D. Ceresoli, M. Cococcioni, N. Colonna, I. Carnimeo, A. D. Corso, S. de Gironcoli, P. Delugas, R. A. DiStasio, A. Ferretti, A. Floris, G. Fratesi, and G. Fugallo et al., "Advanced capabilities for materials modelling with quantum espresso," J. Phys.: Condens. Matter. **29**, 465901 (2017).

[7] H. J. Monkhorst and J. D. Pack, "Special points for Brillouin-zone integrations," Phys. Rev. B **13**, 5188–5192 (1976).